Title
DYNAMICS OF THE REACTION OF N2 WITH H2, D2, AND HD

Authors
Gentry, W.R.
Gislason, E.A.
Mahan, B.H.
et al.

Publication Date
1968-04-01

UCRL-18190
cy. 2

University of California

Ernest O. Lawrence Radiation Laboratory

DYNAMICS OF THE REACTION OF N_2^+ WITH H_2, D_2, AND HD

W.R. Gentry, E.A. Gislason, B.H. Mahan, and Chi-wing Tsao

April 1968

Berkeley, California

DISCLAIMER

Submitted to the Journal of
Chemical Physics

UCRL-18190
Preprint

UNIVERSITY OF CALIFORNIA

Lawrence Radiation Laboratory
Berkeley, California

AEC Contract No. W-7405-eng-48

DYNAMICS OF THE REACTION OF N_2^+ WITH H_2, D_2, AND HD

W. R. Gentry, E. A. Gislason, B. H. Mahan, and Chi-wing Tsao

April 1968

Dynamics of the Reaction of N_2^+ with H_2, D_2, and HD.

W. R. Gentry,* E. A. Gislason, B. H. Mahan, and Chi-wing Tsao

Inorganic Materials Research Division of the Lawrence Radiation Laboratory and Department of Chemistry, University of California, Berkeley, California

Abstract

Product velocity vector distributions have been determined for the reactive and inelastic scattering of N_2^+ by H_2, D_2, and HD. These distributions show that the reaction proceeds by a direct short-lived interaction rather than by a long-lived collision complex. Most products are scattered in the original direction of the N_2^+ projectile at a speed somewhat greater than calculated from the ideal stripping model. The internal excitation of N_2D^+ and N_2H^+ is very high and decreases somewhat with increasing scattering angle. For HD there is an isotope effect that favors N_2H^+ by large factors at small scattering angles, and N_2D^+ by smaller factors at large angles. The N_2^+ scattered from D_2 shows very little elastic component, but does reveal an inelastic process which is probably the collisional dissociation of D_2.

---

*Present address: Department of Chemistry, Mass. Inst. of Tech., Cambridge, Mass.

In an earlier paper[1] we reported measurements of the energy and angular distribution of products from the reaction of N_2^+ with H_2, D_2, and HD. Using intensity contour maps that show the complete product velocity vector distribution, we were able to demonstrate that the most probable reactive process is one in which the N_2H^+ or N_2D^+ is scattered forward, that is, in the original direction of the N_2^+ projectile. Over a considerable range of projectile energies, the most probable velocity of the forward scattered product is close to, but slightly greater than, that predicted by using the ideal stripping model for the reaction, as has been noted by other investigators.[2-5] However, we also observed product scattered through angles as large as 180° in the center of mass system, and this large angle scattering became relatively more important as the projectile energy was increased. Thus, in addition to the stripping process, "rebound" reactive scattering occurs. In this paper we report further observations of the reactive scattering, and the first description of the nonreactive scattering of N_2^+ by isotopic hydrogen molecules.

EXPERIMENTAL

The instrument used in this work[6] consists of a magnetic mass spectrometer for preparation of a collimated beam of primary ions of known energy, a scattering cell to contain the target gas, and an ion detection train made up of an electrostatic energy analyser, a quadrupole mass filter, and an ion

counter. These major components are described below in more detail.

PRIMARY ION SPECTROMETER

Ions were formed in an electron bombardment source of the type described by Carlson and Magnuson.[7] In this source electrons from a tungsten filament oscillate along the axial direction of a cylindrical collision chamber which is surrounded by a solenoidal magnet. Ions are extracted axially through a circular hole, and pass through aperture lenses which produce an approximately parallel ion beam of circular cross section. At this point the ions can be accelerated or retarded to an energy suitable for magnetic momentum analysis. A quadrupole lens pair then focuses this beam onto the entrance slit of a magnetic momentum analyser. The analyser magnet was designed with the aid of the instrument described by Walton[8] to give high order focusing of the ion beam. The object and image distances are 12 and 24 cm, slit widths 2 mm, and the ion deflection angle 66°.

From the exit slit of the mass spectrometer the ions pass through a quadrupole lens pair which makes the beam parallel and restores it to a nearly circular cross section. After the quadrupole lens, ions are retarded or accelerated to their final energy, and pass through an einzel lens and exit aperature before impinging on the entrance of the collision cell.

VACUUM CHAMBER AND COLLISION CELL

The collision cell is located in the center of a large vacuum chamber which is evacuated by two 6" oil diffusion pumps equipped with liquid nitrogen cooled baffles. Inside the chamber is a large cylindrical copper cold shield that can be cooled by liquid nitrogen. On the top of the chamber is a 24" dia rotatable lid mounted on ball bearings and made vacuum tight by a differentially pumped double Tec-Ring seal.[9] The exit aperture of the collision cell and the entire detection train are mounted on this lid and rotate with it.

The collision cell consists of two concentric cylinders. The inner cylinder is held stationary and contains the ion beam entrance aperture (2 × 2 mm) while the outer cylinder contains the product ion exit aperture (2 mm dia) and rotates with the detection train. This exit aperture can be positioned in a range of ± 55° from the projectile beam direction. The conductance of the apertures is small enough and the seals between the cylinders good enough that it is possible to maintain a pressure in the main vacuum chamber which is a factor of 10^3 smaller than the collision cell pressure. The distances of the entrance and exit apertures from the center of the scattering cell are 1.60 and 2.24 cm, respectively.

DETECTION TRAIN

Ions leaving the collision cell pass into a 90° spherical electrostatic energy analyser. The exit aperture of the collision cell and entrance aperture of the analyser provide an angular resolution of 2.5° geometric full width, while the

entrance and exit apertures of the analyser give an energy resolution of 3% FWHM of the analysis energy.

The 90° deflection produced by the analyser directs the ions into a vertical trajectory through a series of cylindrical lenses which focus the ions into a quadrupole mass filter. The axis of the mass filter can be floated at a DC level up to several hundred volts, which makes it possible to mass analyse the ions at an axial kinetic energy of 15 volts. Optimum focusing voltages for the experimental range of ion energies were determined and tabulated for use. The transmission of the lens-mass analyser system was found to be nearly constant in this range of ion energies.

After leaving the mass filter, ions strike a highly polished aluminum surface which is maintained at approximately -25 KeV. The secondary electrons released by the ion impact then impinge at 25 KeV energy on a lithium drifted silicon wafer which is the sensing element of the counting system. The semiconductor detector, FET preamplifier, and linear amplifier have been described in detail by Goulding,[10] and Goulding and Landis.[11] A Hamner Model NS-11 timer, two NT-16 10 Mc scalers, a NE-11 scanner, a NR-10 ratemeter, and a Model 33TC teletype-writer complete the counting system.

DATA ACQUISITION

Experiments were performed by selecting primary ions of the desired energy, adjusting the focusing to give a beam of maximum intensity, stability, and of optimum energy and angular

shape. With the quadrupole mass spectrometer set for the appropriate mass, scans of intensity as a function of product energy were made by determining the counting rate at a series of energy selector and focusing potentials. Scans of the angular distribution at constant energy required no adjustment of the focusing potentials and were made simply by rotating the lid on which the detection train was mounted. The primary beam intensity was checked at intervals of 10-30 minutes, and linear interpolation of any drift was used to calculate the beam intensity corresponding to each data point taken in the time interval.

Because of the favorable ratio of scattering cell to background pressure, the number of product ions formed outside the scattering volume which reached the detector was negligible except when the detector was set at very small angles with respect to the primary beam. This background contribution was determined by noting the pressure in the main chamber with gas in the scattering cell, then evacuating the scattering cell and leaking target gas into the main vacuum chamber until the background pressure was restored, and then measuring the counting rate.

RESULTS AND DISCUSSION

Figure 1 shows typical primary data taken in energy and angular scans of the beam and product distribution. The energy scan was made with the detector aligned with the primary N_2^+ beam direction ($\Theta = 0°$ laboratory) and the intensity maxima at high and low energy correspond to scattering through angles

of $\theta = 0°$ and $180°$, respectively, in the center of mass coordinate system. The angular scan of product intensity shown in Fig. 1b was made at an energy that corresponds to the center of mass velocity of the N_2^+-D_2 system. Thus the two peaks observed at $\pm 5°$ in the laboratory coordinate system correspond to scattering through $\pm 90°$ in the center of mass system. Contour maps of scattered intensity were constructed by reading off the energies and angles corresponding to particular intensities from many such intensity profiles.

The maps here and in our earlier publication[1] show contours of constant intensity per unit velocity space volume. It can easily be shown that this intensity is independent of the coordinate system used to describe the scattering. Particle flux into a differential volume of velocity space must be conserved, thus

$$I_{lab}(\Theta,\Phi,v)v^2dv\ \sin\Theta d\Theta d\Phi = I_{CM}(\theta,\phi,u)u^2du\ \sin\theta d\theta d\phi,$$

where (Θ,Φ) and v are the scattering angles and speed in the laboratory coordinate system, θ, ϕ, and u are the corresponding quantities in the center of mass system. Since the volume elements in the two systems are the same, I_{lab} and I_{CM} are equal. They are related to the differential cross section per unit speed, I'_{lab} and I'_{CM}, used by Herschbach et al[12] by the following equations:

$$I'_{lab}(\Theta,\Phi,v) = v^2 I_{lab}(\Theta,\Phi,v)$$

$$I'_{CM}(\theta,\phi,u) = u^2 I_{CM}(\theta,\phi,u)$$

On the other hand, theoretical treatments of scattering generally yield $I_n(\theta,\phi)$ defined as the number of particles in the state n reaching the detector per unit time per steradian. The relationship between $I_n(\theta,\phi)$ and $I_{CM}(\theta,\phi,u)$ is

$$I_n(\theta,\phi)(dn/du) = I_{CM}(\theta,\phi,u)u^2$$

where dn/du represents the number of internal states of the product per unit speed in the center of mass system.

The actual intensity plotted in the maps is not $I_{CM}(\theta,\phi,u)$, of course, but this quantity averaged over the detector volume. The number of counts per second at the detector C were converted to normalized relative intensities $\bar{I}$ using the expression

$$\bar{I} = \bar{I}_{CM}(\theta,\phi,u) = \bar{I}_{lab}(\Theta,\Phi,v) = 10^7 C/[i_o P g(\Theta)(0.44\ E_f)^{3/2}],$$

where i_o is the peak incident beam intensity in units of 10^{-12} amps, P is the scattering gaspressure in units of 10^{-4} torr, $g(\Theta)$ is the fraction of the scattering volume subtended by the detector at the laboratory scattering angle Θ, and E_f is the final laboratory energy of the ion. The factor $E_f^{3/2}$ normalizes the intensity to the detection volume in velocity space, which increases as $E^{1/2}$ due to the transmission band of the energy analyzer and as E_f due to the v^2 factor in the velocity volume element.

In our experiments $\bar{I}$ is the most convenient representation of our data for a number of reasons. It is better than the raw counts per second since it is normalized to standard values of several widely varying experimental parameters such as beam

intensity, scattering gas pressure, and detector passband. Yet it is still a straightforward presentation of the intensities as measured in the laboratory. Provided the spread in initial relative velocities is small and $I_{CM}(\theta,\phi,u)$ is slowly varying over the detector volume $\bar{I}$ is also a very good approximation to $I_{CM}(\theta,\phi,u)$. This is an advantage over plotting I'_{lab} (which is not equal to I'_{CM}), since we are ultimately interested in intensity distributions in the center of mass systems. When the above conditions are not met, however, the experimental data will not directly yield intensities in the center of mass system. Thus any attempt to plot I'_{CM} will require assumptions about $I_{CM}(\theta,\phi,u)$ or the initial relative velocity spread which are not directly available from the data. So neither I'_{CM} nor I'_{lab} is satisfactory under all conditions while $\bar{I}$ is, and we have used this cross section in all our contour maps.

From $\bar{I}$ it is possible to calculate the angular distribution function or differential cross section in the center of mass system $I(\theta)$ by

$$I(\theta) = \int_0^\infty \bar{I}(\theta,\phi,u)u^2 du. \qquad (1)$$

This differential cross section is still dependent on the initial kinetic energy, as is the total reaction cross section σ given by

$$\sigma = 2\pi \int_0^\pi I(\theta) \sin\theta d\theta \qquad (2)$$

We have calculated both these quantities numerically from $\bar{I}(\theta,u)$.

Figures 2 and 3 show product intensity distributions $\bar{I}$ of N_2H^+ from the N_2^+-H_2 reactant at 5.6 eV relative energies, and of N_2D^+ from the N_2^+-D_2 reaction at 11.2 eV relative energy. These distributions and the ones reported previously[1] show a very pronounced peaking of intensity at zero angle in the center of mass system. The asymmetry of the distributions about $\theta = \pm 90°$ shows that the reaction proceeds by a direct or short-lived interaction, rather than by an intermediate complex that lives as long as a few rotational periods. The predominance of the forward scattering indicates that a projectile N_2^+ can with high probability pick up a hydrogen atom and continue on a nearly straight line path, imparting little if any transverse momentum to the free hydrogen atom.

While small angle scattering predominates, reaction products are observed at all angles in the center of mass system. Consequently, "rebound" processes occur in which the N_2H^+ product acquires a velocity component in the center of mass system opposite to the direction of approach of the N_2^+ projectile, and the free hydrogen atom receives considerable momentum. For large relative energies, a slight peaking in the angular distribution of product intensity appears at $\theta = 180°$. This backward peak is not evident for the N_2^+-H_2 reaction at 5.6 eV relative energy, as Fig. 2 shows, but is obvious for the same reaction at 8.1 eV relative energy,[1] as well as for the N_2^+-D_2 reaction[2] at 8.1 eV, and, as Fig. 3 shows, at 11.2 eV.

The significance of the product intensity distributions becomes clearer if we introduce the translational exothermicity of the reaction Q, which is defined by

$$Q = \frac{\mu' g'^2}{2} - \frac{\mu g^2}{2}$$

Here μ and g are respectively the reduced mass and relative speed of the reactants, and the primed quantities refer to the products. By assuming the reactants are in their ground states we can also write

$$Q = -\Delta E_0^\circ - U$$

$$Q(eV) = -2.5 + D(N_2\text{-}H^+) - U$$

where ΔE_0° is the energy change for the reaction, U is the internal excitation energy of the products, and $D(N_2\text{-}H^+)$ is the unknown dissociation energy of N_2H^+ into a proton and a nitrogen molecule. The range of possible values of Q is limited by the value of ΔE_0° and the expectation that the products are unstable and undetectable if $U > D$. Thus

$$-2.5 \leq Q \leq -\Delta E_0^\circ$$

The lower limit for Q is rigorously specified except for the possibility that metastable N_2H^+ might live long enough (30 μsec) to reach the detector. The upper limit can only be estimated since ΔE_0° is unknown. An upper limit of zero for ΔE_0° can be deduced from the fact that the reaction between N_2^+ and H_2 is rapid even at thermal energies, and thus is very probably not endothermic. In addition, analogy to the isoelectronic molecule HCN suggests that the dissociation energy of N_2H^+ to N_2^+ and a hydrogen atom could be as high as 5.5 eV, which would correspond to a dissociation energy to N_2 and H^+

of 3.5 eV, and a value of -1 eV for ΔE_0^o. This estimate gives us a reasonable, if very approximate, estimate of 1 eV for the upper limit of Q.

The velocities of N_2H^+ relative to the center of mass that correspond to values of Q outside the allowed range are indicated by the shaded areas in Fig. 2. Such excluded regions of velocity space could have been indicated in Fig. 3, but due to high projectile energy and consequent very low product intensity, the data in Fig. 3 show enough asymmetry about the direction of the initial relative velocity vector to make comparison of the distribution to the allowed values of Q relatively uninformative.

From Fig. 2 we see that a certain amount of product intensity appears at values of Q greater than 1 eV, a region nominally excluded by energy conservation. This apparent discrepancy may be a result of an underestimate of $D(N_2\text{-}H^+)$, or may indicate that an important fraction of reactant ions are in excited vibrational and electronic states. However, Moran and Friedman[13] estimate from overlap integral calculations that 90% of the N_2^+ ions formed by electron impact in the $X^2\Sigma_g^+$ state are in the ground vibrational level. It has also been suggested that as much as 10% of the ions may be in the $A^2\Pi_u$ state (excitation energy 1.12 eV) as long as 1-10 μsec after formation by electron impact. In our apparatus the 30 μsec flight time from the extraction aperture to the collision cell, plus the undetermined time spent in the ionization chamber before extraction should reduce the fraction of ions in the

$A^2\Pi_u$ state below 10%. Thus while it is not possible to rule out the presence of the excited electronic state, it would appear to be of minor importance.

It is likely the appearance of products in excluded regions of velocity space is a consequence of finite instrumental resolution combined with the motion of the target hydrogen molecules. Although the angular resolution in the laboratory coordinate system is better than 2°, it is no better than 35° in the center of mass system for N_2^+-H_2 collisions. This factor could be responsible for the intensity in regions around $|\theta| = 45°$ and $Q > 1$ eV in Fig. 2.

Even if the initial and final ion velocities could be measured exactly, the values of Q deduced are somewhat uncertain due to target motion. The error in Q arising from target motion is found to be

$$\delta Q = 2v_H[Mv_i - (M+m)v_f] + mv_H^2$$

where M and m are the masses of the nitrogen molecule and abstracted hydrogen atom, v_i and v_f are the initial projectile and final product velocities, and v_H is the thermal velocity of the abstracted hydrogen atom. It is of interest to note that the uncertainty in Q vanishes to first order in the target velocity for the ideal stripping process, since in this case v_f equals $Mv_i/(M+m)$. For other combinations of v_i and v_f, the uncertainty in Q may be of the order of 0.2-0.3 eV. Finite energy resolution introduces an additional uncertainty of 0.2 eV. The combination of finite energy and angular resolution

together with target motion seem sufficient to rationalize the presence of some scattered intensity in regions of velocity space corresponding to $Q > 1$ eV or $Q < -2.5$ eV.

Despite the uncertainties imposed by finite resolution and target motion, it is possible to make some general observations concerning the amount of the internal energy in the ion product. Figure 2 shows that for N_2H^+ scattered in the forward direction, the highest intensity appears at $Q = -2.5$ eV, which corresponds to products excited internally to levels very near the dissociation limit. For products scattered through angles of 90° or greater, the maximum intensity appears at an appreciably larger value of Q, approximately -1.7 eV. Such a Q value indicates that the backscattered ions are internally excited, but to a noticeably smaller degree than products scattered forward. Apparently the recoil naturally associated with backscattering can lower the internal excitation of the ions somewhat, whereas recoil and product stabilization is accomplished less easily in the grazing reactive collisions associated with forward scattering.

In the analysis of the reaction of potassium with bromine, Berstein and coworkers[14] assumed that the distribution of product internal energy was independent of scattering angle θ. While this assumption appears to be valid for the data available for the $K + Br_2$ system, it is clearly not valid for the $N_2^+ + H_2$ reaction. It must be emphasized, however, that the systems are quite different, since in our experiments the relative

kinetic energy is greater than the exothermicity of reaction, whereas the opposite is true for the $K + Br_2$ system.

Several groups[2,4,5] as well as ourselves[1] have discussed the significance of the velocity of the forward scattered product. Here we only comment that for relative collision energies greater than about 5 eV, the most probable laboratory velocity for forward scattered products is greater than the value predicted by the ideal stripping model. The reason for this is apparent from Fig. 2. Even at 5.1 eV relative energy the maximum in forward intensity lies at $Q = -2.5$ eV, the most negative value consistent with stable products. At higher relative energies, forward recoil and concommitant deviations from the ideal stripping model are necessary if stable products are to be formed.

The slight intensity peaking at $\theta = 180°$ that is evident in Fig. 3 as well as the maps from other high energy experiments requires comment. In the case of elastic scattering of atoms, such backward glory scattering implies that orbiting collisions occur in which the particles remain close for at least one rotational period. It is not necessary to postulate such long-lived intermediates to explain a backward glory in molecular reactive scattering. Peaking at $\theta = 180°$ can occur whenever it is possible for collisions with a nonzero impact parameter to lead to backward reactive scattering. One of several types of collision that could produce backward peaking is the ideal knockout process. In this case the N_2^+ would collide impulsively

with one hydrogen atom so as to eject it from the molecule, and then pick up the remaining hydrogen atom to form N_2H^+. Such a process would produce backscattered ions, and would occur with greatest probability when the axis of the hydrogen molecule was oriented perpendicular to the projectile trajectory and the impact parameter was approximately equal to half the bond distance.

The kinematics of the ideal knockout process lead to the prediction that for 180° scattering the ratio of the product laboratory velocity to the velocity of the projectile is given by

$$\frac{v_f}{v_i} = \frac{M\,(M-m_2)}{(M+m_1)(M+m_2)}$$

where M is the projectile mass, m_2 is the mass of the ejected target atom, and m_1 is the mass of the target atom in the product. Thus the velocity ratio should depend only on the masses of the atoms, according to this model.

It is also possible to calculate the internal excitation energy of the product. According to the knock-out model, this should be the sum of the exothermicity of the reaction and the kinetic energy of the projectile relative to abstracted atom after the projectile has made an elastic collision with the ejected atom. The result is

$$U = -\Delta E_0^o + \left(\frac{Mm_1}{M+m_1}\right)\left(\frac{M-m_2}{M+m_2}\right)^2 \frac{v_i^2}{2} \qquad (3)$$

If U is greater than D, the smallest bond dissociation energy of the product, the product ions will be unstable, and none

will reach the detector. Thus, after substituting D for U, Eq. (3) can be solved for a critical projectile velocity above which no backscattered product should be detected. This critical velocity is higher the smaller the mass of the abstracted atom, and the closer the masses of the projectile and ejected atom. In their discussion of the kinematics of the knock-out process, Light and Horrocks[15] omit the important term ΔE_0^o in Eq. (3) and are led to an overestimate of the critical velocity for exothermic reactions.

Figure 4 shows a comparison between the experimental velocity ratios v_f/v_i for product scattered through 180°, and the predictions of the ideal knockout model. Also shown are the velocity ratios that correspond to the limiting Q values of +1.0 and -2.5 eV. The relative energy at which the predicted velocity ratio line intersects the Q = -2.5 eV curve is the critical energy above which the product is unstable, according to the knockout process.

From Fig. 4 it is clear that product is observed from all four isotopic reactions at relative energies well above the maximum values allowed by the knockout process. In particular, for the formation of N_2D^+ from HD, the model suggests no product should have been detected in any of the experiments performed except one. The model gives particularly high product excitation for this reaction because the projectile loses little energy upon elastic collision with the light hydrogen atom, and therefore moves with considerable energy relative to the heavy deuterium atom. The opposite is true

for the formation of N_2H^+ from HD, and Fig. 4 shows that for this case the experimentally observed ratios are close to the values predicted from the knockout model at the lower relative energies.

In general, the experimental laboratory velocity ratios and, equivalently, internal excitation of the product are smaller than predicted from the ideal knockout model. Moreover, there is no evidence of an abrupt product intensity loss above the critical projectile energies derived from the knockout model. These considerations suggest that the ideal knockout model does not provide a good description of the backward scattering. Indeed, it is difficult to imagine the ejection and pick-up of the two hydrogen atoms as separate events, given the sizes and strong long range interaction of N_2^+ and H_2. We know of no other simple model which is successful in predicting final velocities for back scattered products from all four isotopic reactions.

Both the angular distribution of reaction products $I(\theta)$ and the total reaction cross section σ were calculated from the measured $\bar{I}(\theta,u)$ using Eqs. (1) and (2). Because of imprecise pressure calibration and the constant but uncertain transmission factors only the relative values of $\bar{I}$ have meaning, and in order to obtain an absolute reaction cross section it was necessary to scale our calculation to some absolute measurement. We normalized our results for the total cross section of the N_2^+-D_2 reaction at 11.2 eV relative energy to the measurement of Turner et al.[3] at this energy. The two other N_2^+-D_2

experiments for which complete maps of $\bar{I}$ are available then give total cross sections in good agreement with Turner's values.[3]

The angular distribution $I(\theta)$ of total product is shown in Fig. 5 for reactions with H_2 and D_2 calculated from the contour maps in this paper and our earlier work.[1] The angular distributions for the two reactions are very similar at the same relative energy. As the relative energy increases the intensity at all angles decreases, but the peaking at small angles becomes more pronounced. The general shape of these curves is similar to that found by Birely et al.[15] for the reactions of alkali metals with bromine and iodine but is even more sharply peaked at $\theta = 0°$.

The angular distribution curves of Fig. 5 do not show the intensity peak at 180° which is evident in Fig. 3 and the previously published intensity maps.[1] Inspection of the maps shows that the intensity distribution tends to narrow in velocity as well as peak in angle near $\theta = 180°$. Thus it is not surprising that the integrated intensity $I(\theta)$ does not have a maximum at $\theta = 180°$. Given the general character of the product distribution, and the fact that our laboratory speed resolution is usually better than the angluar resolution, it seems possible that some of the backward peaking evident on the intensity maps is an instrumental artifact. In any case failure to observe peaking at 180° in the product angular distribution $I(\theta)$ completely eliminates the possibility that the reaction proceeds through a long-lived collision complex.

No product intensity maps were obtained for the N_2^+-HD reactions, so it is not possible to compute the angular distributions at all angles and total cross sections for these cases. However, in Table I we give our measured values of $\bar{I}$ (peak value) and the computed $I(\theta)$ for $\theta = 0°$, 90°, and 180°. It can be seen that the intensity of N_2H^+ at $\theta = 0°$ greatly exceeds that of N_2D^+ for all initial relative energies, regardless of whether $\bar{I}$ or I are compared. This very large isotope effect favoring hydrogen over deuterium in the forward scattered products largely disappears if $\bar{I}$ or I is plotted as a function of E_a^o, the energy of the projectile relative to the atom abstracted.

Isotope effects similar to these have been observed and discussed in terms of the ideal stripping model by Henglein and coworkers.[16] This model predicts that the internal excitation of the forward scattered product is

$$U = -\Delta E_0^o + \frac{m_1}{M + m_1} E^o \qquad (4a)$$

$$= -\Delta E_0^o + E_a^o, \qquad (4b)$$

where M and m_1 are the masses of the projectile and abstracted atom, and E^o and E_a^o are the projectile energies in the laboratory and relative to the abstracted atom. According to these expressions the internal energy of N_2D^+ will be greater than that of N_2H^+ for any given projectile laboratory energy. An infinite isotope effect is expected for projectile energies

above 37.5 eV, for then U exceeds the dissocation energy of the product for deuterium but not for hydrogen abstraction. Our failure to observe such an infinite isotope effect, together with the observed magnitudes of the product velocities is a clear demonstration that forward recoil and concommitant product stabilization occur, and that the stripping model in its simplest form does not describe the forward scattering quantitatively.

It seems likely, however, that the origin of much of the small angle isotope effects lies in Eq. (4b). In the energy region in which we have done our experiments the intensity of products seems to be chiefly dependent on the amount of energy which must be disposed of. Our experimental observations that most of the products appear sharply peaked at $\theta = 0°$ and that only the minimum momentum necessary for product stability is transferred to the nonreacting atom strongly suggest that the N_2^+ projectile interacts <u>almost</u> exclusively with the abstracted atom. In this case the pertinent relative kinetic energy is E_a^o, the energy relative to the abstracted atoms. If $U > D$, then U-D must be disposed of by recoil of the free atom. This becomes more difficult as E_a^o and thus U grows and the intensity falls sharply.

Henglein's data[17] suggests that an H atom and a D atom are equally effective in disposing of a given energy excess U-D. An examination of our intensity data confirms this over the entire energy range studied by us. We must be cautious, however,

since our contour maps indicate that the scattering near $\theta = 0°$ is more strongly peaked than the pass band of our detector in both velocity and angle. If this is true then $\bar{I}(\theta,u)$ and our computed $I(\theta)$ will be smaller than their true values. However, it can then easily be shown that

$$\sigma_s = I(\theta=0°)(v_{max}/u_{max})^2 \qquad (5)$$

is, apart from a normalizing constant, the total amount of scattering in this region. The factor $(v_{max}/u_{max})^2$ is the square of the ratio of the laboratory velocity of the product at the peak to the center of mass velocity at the peak. It basically converts $I(\theta = 0°)$ to $I(\Theta = 0°)$ so we can make use of the fact that the laboratory angular resolution (but not the center of mass resolution) of the detector is the same for all hydrogen isotopes. The normalizing constant mentioned above will then include the (constant) FWHM laboratory angular resolution. The cross section σ_s can be thought of as the total cross section for stripping. In fact, since our computed $I(\theta = 0°)$, though too small, is still about ten times the values at $\theta = 90°$ and 180° we feel that the normalized σ_s is within experimental error equal to the true total cross section. Once again we have normalized our N_2^+-D_2 result at 11.2 eV relative energy to Turner's result[3] (0.27 Å^2) at the same energy. Figure 6 shows σ_s plotted versus E_a^o for the four possible reactions; the values for HD have been multiplied by 2 since it contains only one H atom compared to two in H_2 and one D atom compared to two in D_2. There is remarkably good

agreement among the four reactions. The total cross section for N_2^+-D_2 measured by Turner[3] have also been plotted along with the curve derived by Henglein[17] from his N_2^+-H_2 and N_2^+-D_2 data, which also gives a reasonably good fit to his HD data. The best fit straight line to our data has a slope $\partial \log \sigma_s / \partial E_a^o = -0.42$ in good agreement with Henglein's value of -0.35 and our estimated value of -0.40 for Turner's data. Figure 6 also gives our total cross sections σ, computed from Eq. (2) as described earlier. The values of σ and σ_s are in satisfactory agreement at all energies.

Product which appears at larger angles in the center of mass involves substantial recoil of the nonreacting H or D atom. We have seen earlier that product at $\theta = 90°$ and 180° is noticeably less excited internally than product at $\theta = 0°$. Both of these facts suggest that the picture of an N_2^+ projectile interacting only with the abstracted atom which is successful at small angles breaks down for products at larger angles. Thus it is not surprising that plots of I (90°) or I (180°) versus E_a^o are no longer the same for the four possible reactions. The relative energy of the projectile and the entire molecule E_s^o now becomes the significant dynamical parameter. The total amount of product $I(\theta)$ produced at $\theta = 90°$ and $\theta = 180°$ is shown as a function of E_s^o in Fig. 7. For HD this involves summing the intensities for N_2H^+ and N_2D^+. All three molecules give about the same exponential dependence of product intensity on E_s^o at both angles, which is in marked contrast to the behavior found at $\theta = 0°$. The fact that intensity decreases as energy

increases may be due to an increase in difficulty of stabilizing product molecules at the higher energies. However, the observation[1] that the most probable product internal excitation energy is below the dissociation limit for large angle scattering suggests other factors may also be important. The most obvious possibility is that for small impact parameter collisions, charge transfer and dissociative charge transfer[18] start to compete significantly with chemical reaction as energy increases.

It is of interest to compare the relative probability of forming N_2H^+ and N_2D^+ from HD at the larger scattering angles. The experimental isotope effect is shown in Fig. 8 for $\theta = 90°$ and 180°. In addition the ratio $\sigma_s(N_2H^+)/\sigma_s(N_2D^+)$ for HD is shown in order to give an indication of the isotope effect at $\theta = 0°$. It is obvious that for high projectile energies there is an enormous isotope effect favoring N_2H^+ at $\theta = 0°$, a similar small effect at $\theta = 180°$, and an intermediate effect at $\theta = 90°$. The decrease in the isotope effect with increasing angle evidently indicates that the energy of the projectile relative to the abstracted atom, or equivalently the internal energy of the incipient N_2H^+ or N_2D^+ becomes less critical as the impulse imported to the freed atom increases. In contrast to the situation that holds for stripping or grazing collisions, in the intimate collisions associated with back scattering the atoms are strongly coupled, and the product internal energy and stability are not closely correlated with isotopic composition. It should be noted that at large angles and low energies there is a relatively small isotope effect that favors N_2D^+

over N_2H^+ from HD. The same phenomena appears when one compares N_2D^+ and N_2H^+ from D_2 and H_2. We have no explanation for this inverse isotope effect. It can be regarded as further evidence against the knockout model, which would predict that the product be dominantly N_2H^+ over the experimental energy range. A similar failure of the knockout model in hot atom reactions has been noted by Cross and Wolfgang.[19]

The nonreactive scattering of N_2^+ by D_2 was investigated using projectile laboratory energies from 25 to 130 eV. In one of these experiments enough energy and angular scans were made to generate the contour map shown in Fig. 9. Three important features are apparent. First, there is no evidence of any elastic scattering at large center of mass angles. In an investigation[20] of collisions of N_2^+ with He, we were able to detect N_2^+ scattered elastically and with some inelastic loss at angles as large as $\theta = 180°$. Consequently, the failure to detect large angle elastic scattering in the N_2^+-D_2 system is not due to lack of sensitivity. We can conclude that in the N_2^+-D_2 system, collisions with small impact parameters lead virtually exclusively to reaction, charge transfer, dissociative charge transfer, or very inelastic nonreactive scattering.

The second feature to be noted from Fig. 9 is the relatively small total intensity of scattered N_2^+ except for the elastic scattering at very small center of mass angles. Together with the low intensity of N_2D^+ found for such high projectile energies, this suggests that most small impact parameter collisions produce neutral nitrogen molecules and

D_2^+ or its dissociation products. This is consistent with the observations of Vance and Bailey[18] that the cross sections for charge transfer with and without dissociation increase with increasing projectile energy, and are of the order of 10 $Å^2$ for 100 eV ions.

The third feature of importance is the peak in the scattered N_2^+ intensity at $\theta = 0°$ and a Q value of -9.5 eV. To find the process responsible for this peak, we determined its intensity profile along $\theta = 0°$ at several projectile energies. The results are displayed in Fig. 10 as plots of P(Q), the probability of finding a given value of Q, as a function of the relative energy loss Q. P(Q) is given by

$$P(Q) = [I(\theta,u)u^3]/[2E_s I(\theta)]$$

which follows from the definition

$$P(\theta)dQ = I(\theta,u)u^2du$$

and the fact that

$$(\partial Q/\partial u)_{E_s^o} = 2E_s/u$$

where E_s is the relative translational energy of the product. The inelastic feature first becomes discernable when the relative energy is 5.6 eV. As the relative energy increases, the Q that corresponds to the maximum intensity becomes more negative.

We have evaluated $I(\theta = 0°)$ for this inelastic scattering using Eq. (1). In this case the upper limit for the integral was the value of u for which Q was -4.5 eV. This was a

somewhat arbitrary attempt to eliminate the contribution of the small Q scattering which comes from vibrational and rotational excitation. Since the inelastic feature is so sharply peaked in angle, we again used Eq. (5) to estimate the total cross section σ_s as a function of relative energy. This is shown in Fig. 11. We also computed the integrated total cross section σ using Eq. (1) and (2) from the data used in Fig. 9. The good agreement between σ and σ_s for this experiment suggests that as was true for reactive scattering, σ_s is a good approximation to the total cross section. The cross sections in Fig. 11 show an inelastic threshold near 4.5 eV, and increase from 0.01 Å^2 at 6 eV relative energy to 0.6 Å at 16 eV.

There are three processes which might be responsible for this inelastic peak. One is a stripping collision that produces N_2D^+ with internal excitation sufficiently large so that dissociation to $N_2^+ + D$ occurs. The relative energy threshold for this process is 8.4 eV, however, well above the experimentally observed threshold. Moreover, stripping followed by isotropic dissociation would force the ratio of the final laboratory velocity of N_2^+ to the projectile velocity to be 28/30 = 0.9333 at all projectile energies. Experimentally we find for this ratio

$$v_f/v_o = 0.9462 + 0.000418\ (E^o - 100)$$

over the range of energies studied. Stripping followed by product dissociation may contribute to the inelastic process at high projectile energies, but does not do so at the lower energies.

It is possible that collisional electronic excitation of N_2^+ is responsible for the inelastic peak. Excitation of the $B^2\ \Sigma_u^+$ state of N_2^+ by collisions at energies well below 1 KeV with H_2 and the rare gases has been observed spectroscopically.[21] However, if this were the principal source of inelastic loss, it is not clear why the threshold for excitation should be above 3.2 eV, the excitation energy of N_2^+ $B^2\Sigma_u^+$. In addition, it is difficult to see why there should be a peak in the energy loss spectrum which shifts smoothly to larger energy losses as the projectile energy increases. For example, at 8.1 eV relative energy, the P(Q) curve peaks at Q = -6.5 eV, which does not correspond to any Franck-Condon favored transition to a known state of N_2^+. The fact that we did not observe any inelastic peaks at $\theta = 0°$ in our investigation of N_2^+-He collisions[20] suggests that the peak observed in the N_2^+-D_2 system does not arise from electronic excitation of N_2^+, but is connected with excitation of D_2.

Since the inelastic peak has a threshold near 4.5 eV, we feel that it may be associated with the collisional dissociation of D_2. The phenomenon of a stripping reaction followed by dissociation of N_2D^+ accomplishes this, but as mentioned above, this process has a threshold too high to be consistent with the data at low projectile energy. At relative energies above the critical value for product stability, the ideal knockout process can also lead to collisional dissociation of D_2. However, the critical initial relative energy at which N_2D^+ formed in the knockout process becomes unstable with respect to

N_2^+ and D is 9.6 eV, well above the observed threshold. Thus neither the dissociative stripping nor the knockout process can be fully responsible for the inelastic peak.

Another mechanism for dissociation would be a curve crossing phenomenon in which the reactants, moving on a surface that goes asymptotically to $N_2^+ X\ ^2\Sigma_g^+$ and $D_2\ ^1\Sigma_g^+$, are transferred to the surface which has $N_2^+ X\ ^2\Sigma_g^+$ and $D_2\ ^3\Sigma_u^+$ as its asymptotic states. Such a transition is allowed by spin conservation rules and could have a threshold at 4.6 eV, the dissociation energy of D_2. The process might also be pictured as a nearly vertical excitation to the $^3\Sigma_u^+$ state of a D_2 molecule which had been distorted by some degree to large internuclear separation. At low projectile energies the elongation of D_2 might be great, and transitions to the low energy part of the $^3\Sigma_u^+$ curve of D_2 could occur and lead to Q values not much more negative than -4.6 eV. As the projectile energy increased, the time to distort D_2 would decrease, and the overall process would become more vertical with respect to the D_2 internuclear separation. This would account for the increase in cross section and increase in excitation energy as the projectile energy increases. The Franck-Condon factor for excitation from the vibrational ground state of D_2 to the $^3\Sigma_u^+$ state shows a maximum at 9.5 eV, the observed limiting energy loss, and a shape which roughly approximates the inelastic peak observed in the highest energy experiment. Thus collisional dissociation of D_2 by excitation to its lowest triplet state does provide an adequate, if not proven explanation of the inelastic peak observed for N_2^+.

One other point concerning the inelastic scattering of N_2^+ should be recognized. The ratio of the most probable velocity of the inelastically scattered N_2^+ to the projectile velocity increases linearly with increasing projectile energy. Over much of the projectile energy range, this ratio is greater than the product (N_2D^+) to projectile velocity ratio expected for ideal stripping and is near or equal to the experimentally observed velocity ratio for N_2D^+. Also in this same range of high projectile energies, the inelastic cross section is comparable to or greater than the cross section for formation of N_2D^+. Therefore, in Henglein's experiments[2] in which velocity analysis of the scattered ions was carried out without mass analysis, some or even the major part of the apparent N_2D^+ signal was in fact inelastically scattered N_2^+. This possibility was recognized by Henglein.[2] Since the velocity of scattered N_2^+ and N_2D^+ are similar in the energy range where the inelastic and reactive cross sections are comparable, the ambiguity has rather little effect on the velocity ratios determined by Henglein. However, because of the increasing contributions of inelastic scattered N_2^+, Henglein's apparent total reaction cross section decreases with increasing projectile energy somewhat more slowly than the cross section found by ourselves and by Turner et al.[3] In fact, by combining the reactive and inelastic cross sections from Figs. 6 and 10 we predict that the logarithm of the cross section measured by Henglein should decrease linearly with a slope $\partial(\log \sigma_s)/\partial E_a^o =$

-0.33, which is in close agreement to his measured value of -0.35.

SUMMARY

We have used several representations of measured reactive and inelastic scattering to study the qualitative features of the N_2^+-H_2 reaction dynamics. From the velocity vector distributions $\bar{I}(\theta,\phi,u; E^o)$ we learned that the reaction proceeds by a direct interaction mechanism, that the internal excitation energy of the products is a function of their scattering angle, and that most products are scattered in the original direction of the N_2^+ projectile at a speed somewhat greater than that predicted from the ideal stripping model. Velocity ratio plots showed that the ideal knockout mechanism fails to give a quantitative explanation of the velocity or occurrence of back scattered products. From the differential reaction cross section $I(\theta; E^o)$ we drew further support for the direct interaction mechanism, and the predominance of forward scattering. The isotopic variation of this differential cross section at three angles and its dependence on projectile energy showed that the degree to which the reaction product can be stabilized through recoil may in large measure account for observed isotope effects. The observations that the total reaction cross section falls with increasing projectile energy, and is nearly the same for different isotopes at the same energy relative to the abstracted atom further reflect the importance of product

stabilization through recoil at high collision energies. From the studies of nonreactive scattering we found an inelastic process which increases in importance with increasing projectile energy. Together with charge transfer and dissociative charge transfer, collisional dissociation is an important channel which competes with chemical reaction at high collision energies. We expect that more detailed conclusions can be drawn about the reaction dynamics when these data are compared to calculated molecular trajectories obtained using trial potential energy surfaces.

Acknowledgement: This work was supported by the U. S. Atomic Energy Commission. We would like to thank Mr. Arthur Werner for his assistance with some of the experiments. E. A. G. acknowledges the support received from an NIH Postdoctoral Fellowship.

Table I

Relative Intensities[a] and Differential Cross Sections.

Expt. No.	E_s^o	$\bar{I}(0°) \times 10^{-3}$	$\bar{I}(90°) \times 10^{-2}$	$\bar{I}(180°) \times 10^{-2}$	$I(0°) \times 10^2$ (Å^2/sr)	$I(90°) \times 10^2$ (Å^2/sr)	$I(180°) \times 10^2$ (Å^2/sr)
			$N_2^+ + D_2 \rightarrow N_2D^+ + D$				
186	8.13	18.7	3.8	7.0	25.7	2.13	1.94
187	3.12	305	64.0	-	154	7.19	2.79
188	4.38	297	41.5	-	198	6.93	2.74
189	9.38	9.8	2.1	3.7	21.3	1.10	1.10
190	3.12	515	-	-	376	52.2	18.3
191	5.62	212	30.7	47.0	180	12.2	9.65
192	6.86	58.7	17.9	21.3	69.7	7.50	5.12
193	11.23	4.5	50	0.97	8.97	0.468	0.326
			$N_2^+ + H_2 \rightarrow N_2H^+ + H$				
194	2.33	1220	-	-	220	39.6	18.3
195	5.62	114	26.0	25.3	44.2	4.83	2.63
196	4.67	132	44.0	34.5	39.6	5.40	3.31
197	7.35	29.5	8.20	9.50	16.7	2.16	1.32
198	8.92	11.2	3.35	5.90	8.94	1.15	0.993
199	3.13	450	-	130	94.3	27.9	8.18
200	8.11	19.8	6.80	9.40	12.6	2.14	1.45
			$N_2^+ + HD \rightarrow N_2D^+$				
207a	4.34	111	75.3	69.0	27.9	5.53	5.18
208a	5.79	36.5	17.5	42.0	14.1	2.16	3.77
210a	7.25	7.53	3.58	11.0	4.09	0.710	1.30
211a	8.70	2.48	1.00	5.20	2.04	0.318	0.590
212a	10.2	0.72	0.42	1.88	0.906	0.187	0.302
213a	11.6	0.27	0.16	0.98	0.463	0.222	0.176
214a	3.39	160	-	-	27.0	12.3	6.07

(Continued)

Table I (Continued)

Expt. No.	E_s^o	$\bar{I}(0°) \times 10^{-3}$	$\bar{I}(90°) \times 10^{-2}$	$\bar{I}(180°) \times 10^{-2}$	$I(0°) \times 10^2$ (Å^2/sr)	$I(90°) \times 10^2$ (Å^2/sr)	$I(180°) \times 10^2$ (Å^2/sr)
			$N_2^+ + HD \rightarrow N_2H^+ + D$				
207b	4.34	513	13.6	15.7	378	2.85	2.64
208b	5.79	323	5.38	7.20	292	1.59	1.66
210b	7.25	174	2.70	3.30	196	1.30	0.983
211b	8.70	53.5	1.88	1.83	79.9	1.37	0.675
212b	10.2	14.9	0.98	0.87	30.2	0.873	0.335
213b	11.6	8.0	0.58	0.50	18.2	0.652	0.242
214b	3.39	413	-	-	240	6.45	3.18

a. Arbitrary Units.

References

1. W. R. Gentry, E. A. Gislason, Y. Lee, B. H. Mahan, and C. Tsao, Disc. Faraday Soc. 44, 137 (1967).
2. K. Lacmann and A. Henglein, Ber. Bunsenges, Physk. Chem. 69, 279 (1965).
3. B. R. Turner, M. A. Fineman, and R. F. Stebbings, J. Chem. Phys. 42, 4088 (1965).
4. L. Doverspike, R. Champion, and T. Bailey, J. Chem. Phys. 45, 4385 (1966).
5. Z. Herman, J. Kerstetter, T. Rose, and R. Wolfgang. J. Chem. Phys. 46, 2844 (1967); Disc. Faraday Soc. 44, 000 (1967).
6. W. R. Gentry, University of California Lawrence Radiation Laboratory Report UCRL-17691.
7. C. E. Carlson and G. D. Magnuson, Rev. Sci. Inst. 33, 905 (1962).
8. E. T. S. Walton, Proc. Roy. Irish. Acad. 57, 1 (1954).
9. D. Armstrong and N. Blais, Rev. Sci. Inst. 34, 440 (1963).
10. F. S. Goulding, Nuclear Instr. and Methods 43, 1 (1966).
11. F. S. Goulding and D. Landis, Instrumentation Techniques in Nuclear Pulse Analysis, National Academy of Sciences--National Research Council Publication 1184.
12. W. B. Miller, S. A. Safron, and D. R. Herschbach, Disc. Faraday Soc. 44, 000 (1967).
13. T. F. Moran and L. Friedman, J. Chem. Phys. 42, 2391 (1965).

References (Continued)

14. T. T. Warnock, R. B. Bernstein, and A. E. Grosser, J. Chem. Phys. 46, 1685 (1967).

15. J. C. Light and J. Horrocks, Proc. Phys. Soc. (London) 84, 527 (1964).

16. J. Birely, R. Herm, K. Wilson, and D. Herschbach, J. Chem. Phys. 47, 993 (1967).

17. A. Henglein, K. Lacman, and B. Knoll, J. Chem. Phys. 43, 1048 (1965).

18. D. W. Vance and T. L. Bailey, J. Chem. Phys. 44, 486 (1966).

19. R. J. Cross and R. Wolfgang, J. Chem. Phys. 35, 2002 (1961).

20. W. R. Gentry, E. A. Gislason, B. H. Mahan, and C. W. Tsao, J. Chem. Phys. 47, 1856 (1967).

21. C. Liu and H. P. Broida, Bull. Am. Phys. Soc. 13, 448 (1968).

Figure 1. Profiles of the N_2^+ beam and N_2D^+ product distributions. (a) A scan along the direction of the projectile beam ($\Theta = 0°$). The intense, high energy product peak represents forward scattering, and the weaker low energy peak is product scattered through $\theta = 180°$. (b) The N_2^+ and N_2D^+ intensities as a function of the laboratory angle Θ. The scan of the product was made at an energy which corresponds to the center of mass velocity, so the two peaks represent product scattered through $\pm 90°$ in the center of mass system. In both plots the N_2^+ beam intensity has been greatly reduced to make it comparable to product intensities.

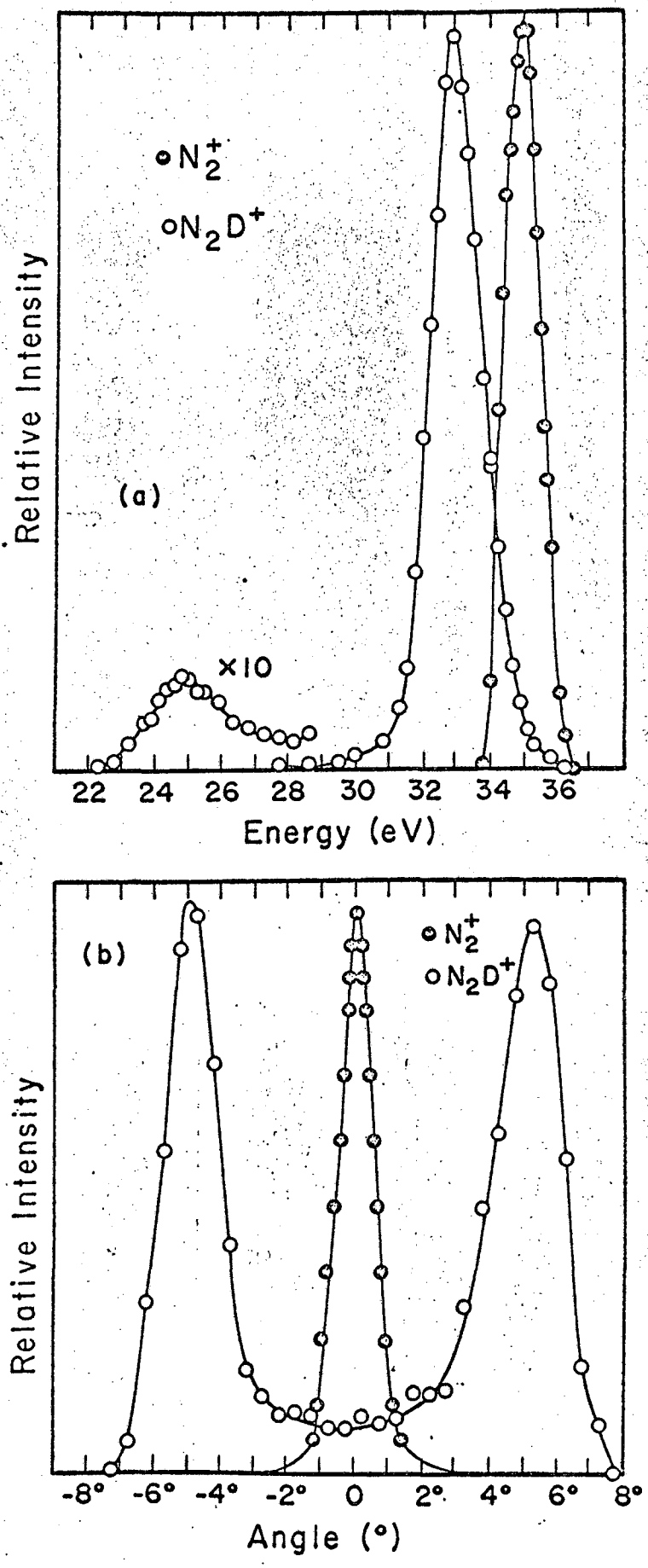
Relative Intensity
$\circ N_2^+$
$\circ N_2D^+$
(a)
×10
22 24 26 28 30 32 34 36
Energy (eV)
(b)
$\circ N_2^+$
$\circ N_2D^+$
Relative Intensity
-8° -6° -4° -2° 0 2° 4° 6° 8°
Angle (°)

Fig. 1

Figure 2. A map of $\bar{I}$, the normalized intensity distribution of N_2H^+ in the center of mass coordinate system. The relative energy of N_2^+ and H_2 reactants was 5.6 eV. The outer shaded area represents values of Q greater than +1.0 eV, and in the inner shaded area, Q is less than -2.5 eV. The circled points represent the actual maxima in the intensity which were located in the energy and angular scans.

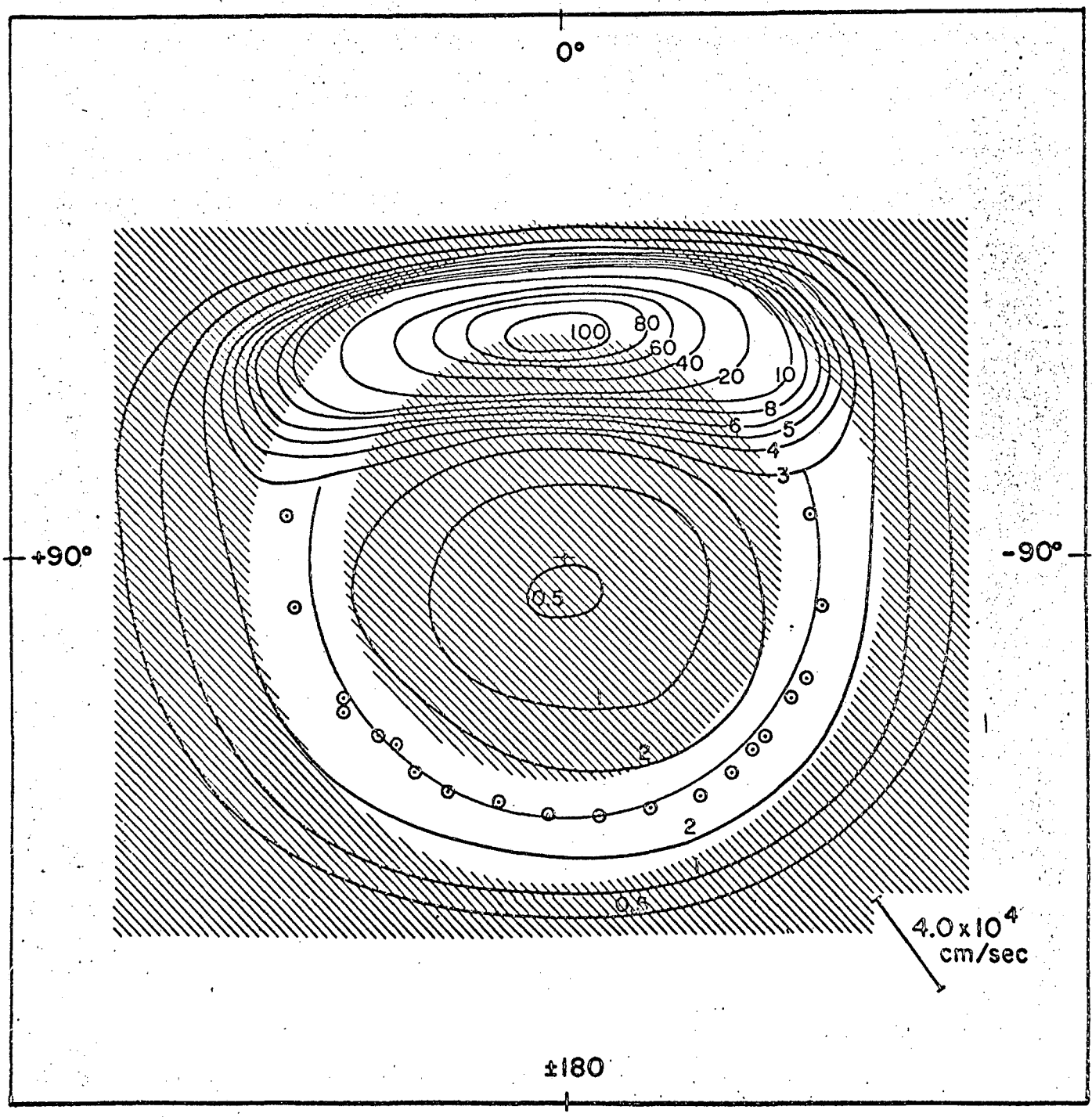
0°
+90°
-90°
±180
100
80
60
40
20
10
8
6
5
4
3
0.5
1
2
0.5
4.0 x 10^4
cm/sec
XBL 678-4796

Fig. 2

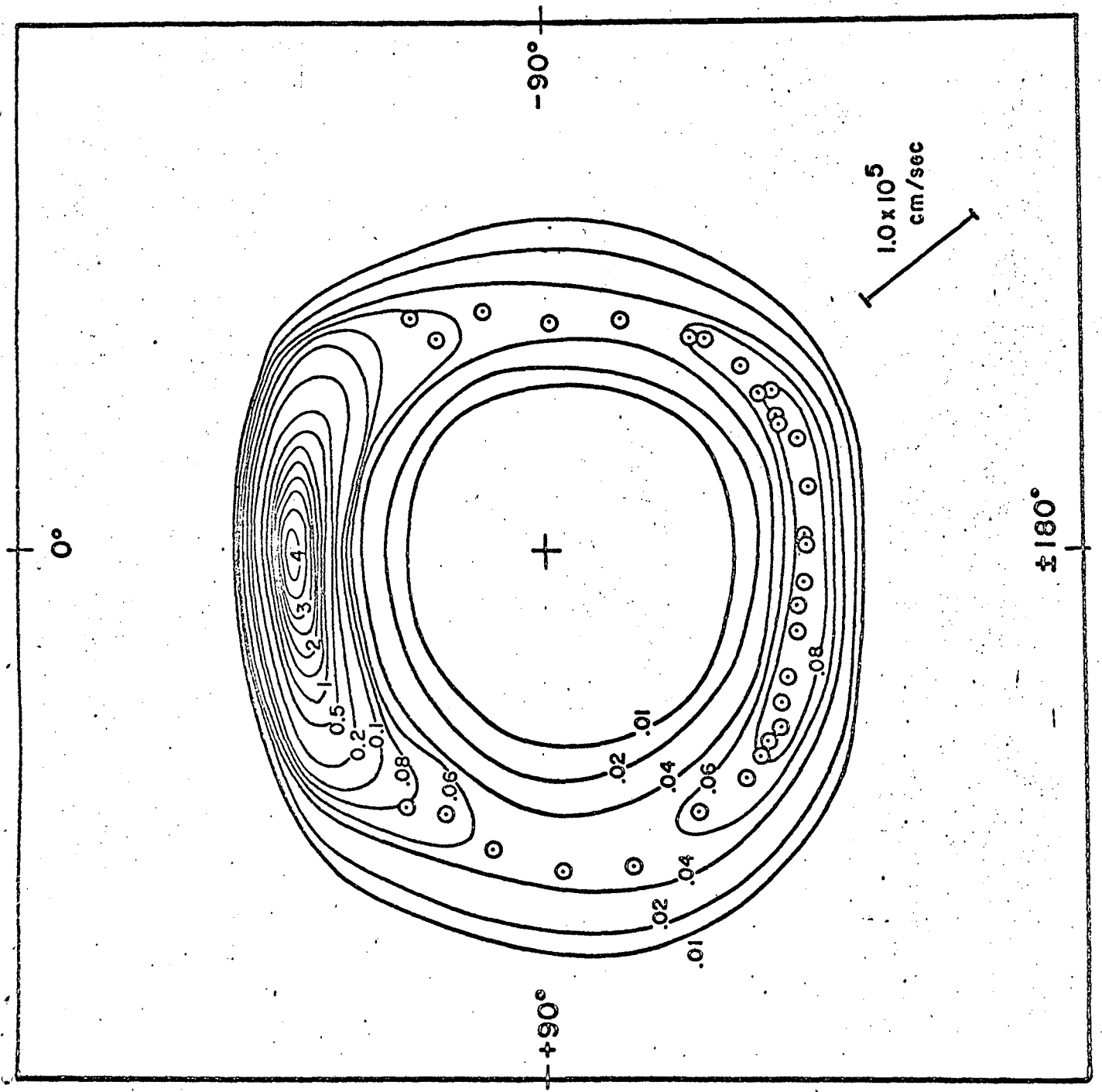

Figure 3. A map of the normalized intensity $\bar{I}$ in the center of mass coordinate system for N_2D^+ from the N_2^+-D_2 reaction at 11.2 eV relative energy.

Figure 4. The ratio of the most probable product laboratory velocity to the projectile velocity as a function of initial relative kinetic energy for products scattered through 180° in the center of mass system. The predictions of the ideal knockout model for each reaction are shown as horizontal dashed lines. The velocity ratios for the limiting Q values of +1.0 and -2.5 eV are also shown.

Fig. 4

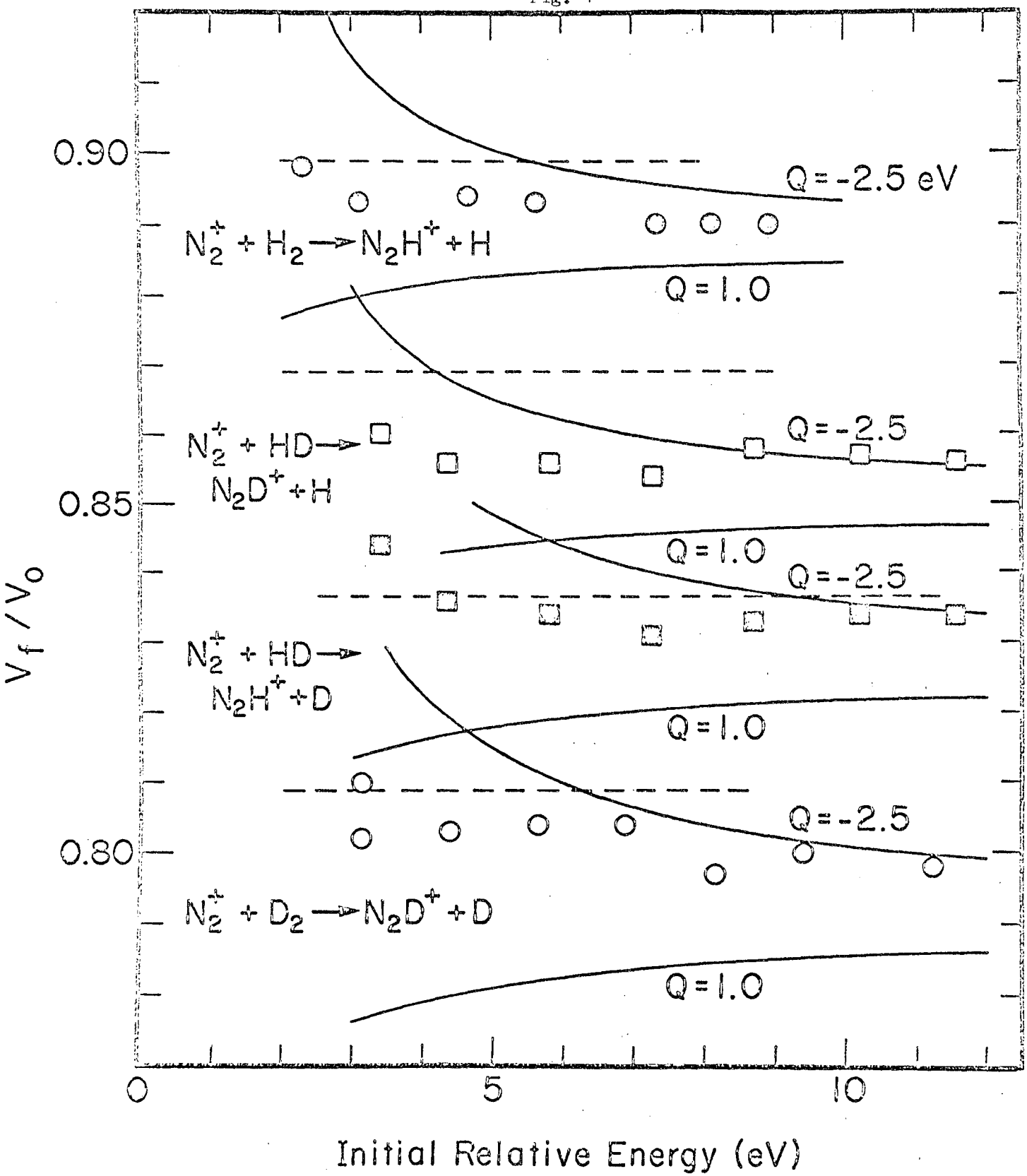
0.90
0.85
0.80
V_f / V_o
$N_2^+ + H_2 \rightarrow N_2H^+ + H$
Q = -2.5 eV
Q = 1.0
$N_2^+ + HD \rightarrow N_2D^+ + H$
Q = -2.5
Q = 1.0
$N_2^+ + HD \rightarrow N_2H^+ + D$
Q = -2.5
Q = 1.0
$N_2^+ + D_2 \rightarrow N_2D^+ + D$
Q = 1.0
0
5
10
Initial Relative Energy (eV)

Figure 6. Total reaction cross sections computed using Eq. (2) (triangles) and Eq. (5) (circles and squares). The results of Turner et al.[3] and Henglein[2] are indicated by the dashed and solid lines, respectively.

Fig. 6

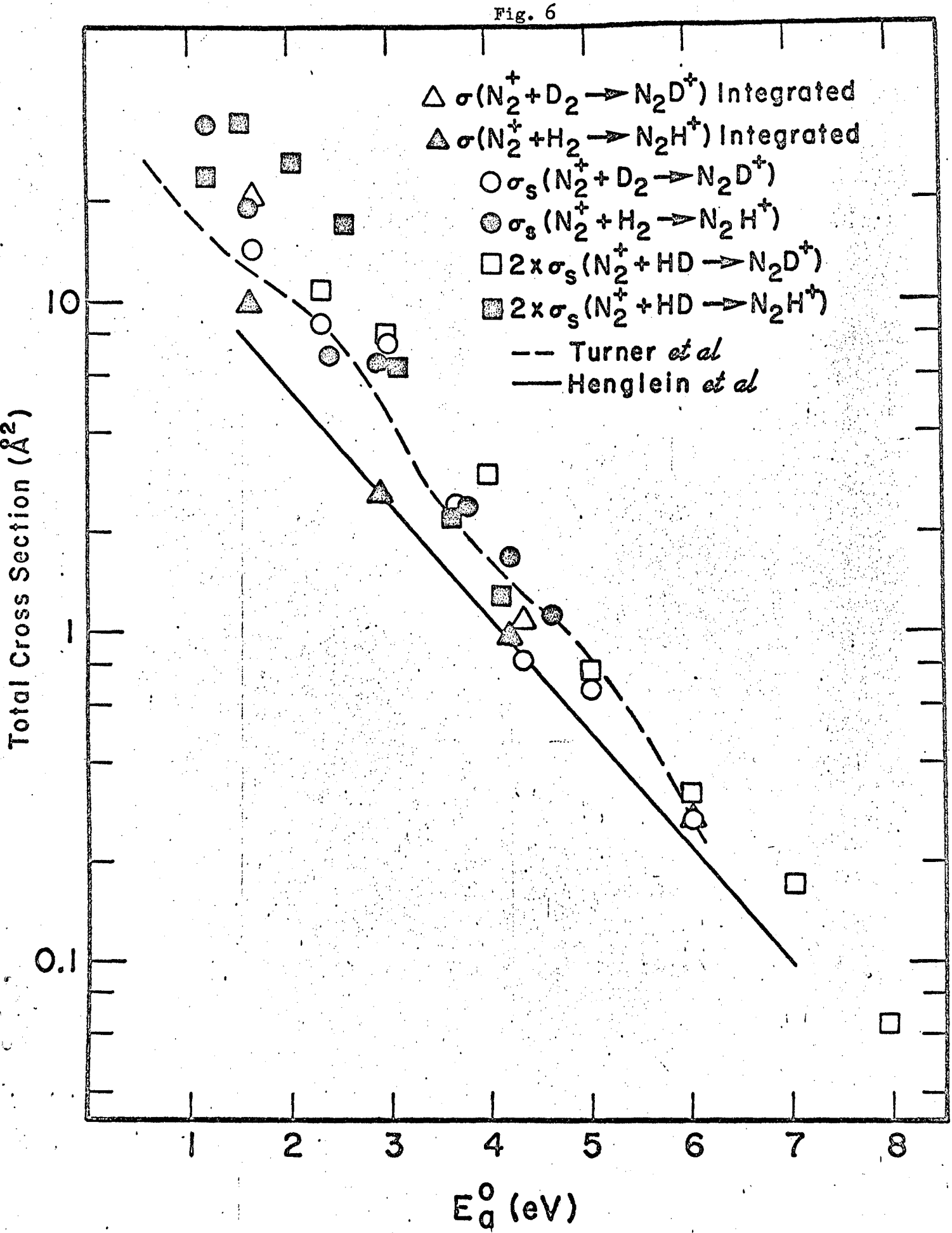
△ σ(N2+ + D2 → N2D+) Integrated
△ σ(N2+ + H2 → N2H+) Integrated
○ σs(N2+ + D2 → N2D+)
● σs(N2+ + H2 → N2H+)
□ 2 x σs(N2+ + HD → N2D+)
■ 2 x σs(N2+ + HD → N2H+)
-- Turner et al
—— Henglein et al
Total Cross Section (Å2)
10
1
0.1
1
2
3
4
5
6
7
8
E°q (eV)

Figure 7. Differential reactive cross sections at $\theta = 90°$ and 180° as a function of energy of the projectile relative to the molecule. For HD, both isotopic products are included. Note the broken scale.

Fig. 7

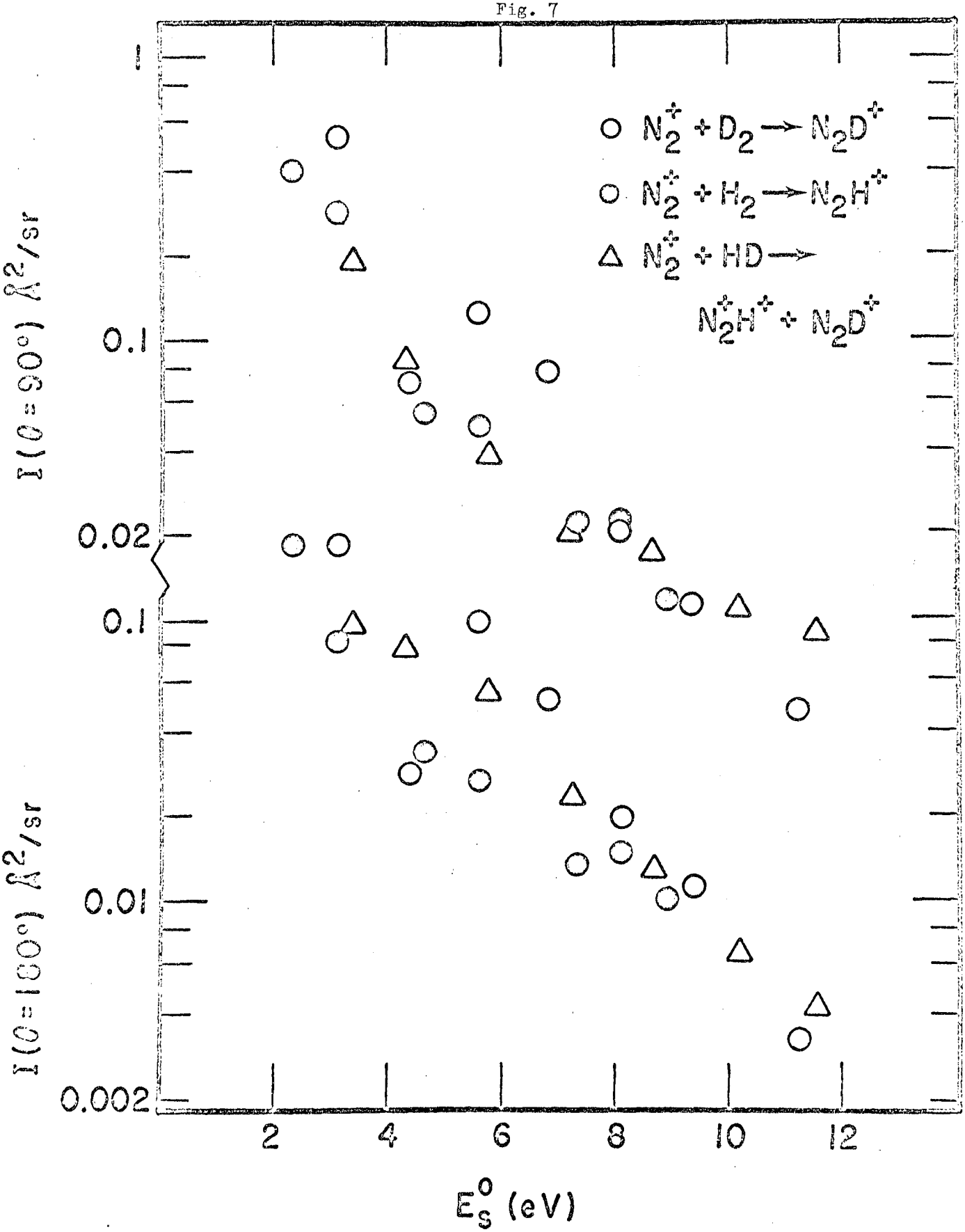
$N_2^+ + D_2 \rightarrow N_2D^+$
$N_2^+ + H_2 \rightarrow N_2H^+$
$N_2^+ + HD \rightarrow$
$N_2H^+ + N_2D^+$
$I(\theta = 90°)$ Å^2/sr
$I(\theta = 180°)$ Å^2/sr
0.1
0.02
0.1
0.01
0.002
2
4
6
8
10
12
E_s^0 (eV)

Figure 8. Isotope effects in the differential and total cross sections for the N_2^+-HD reaction as a function of relative collision energy and scattering angle.

Fig. 8

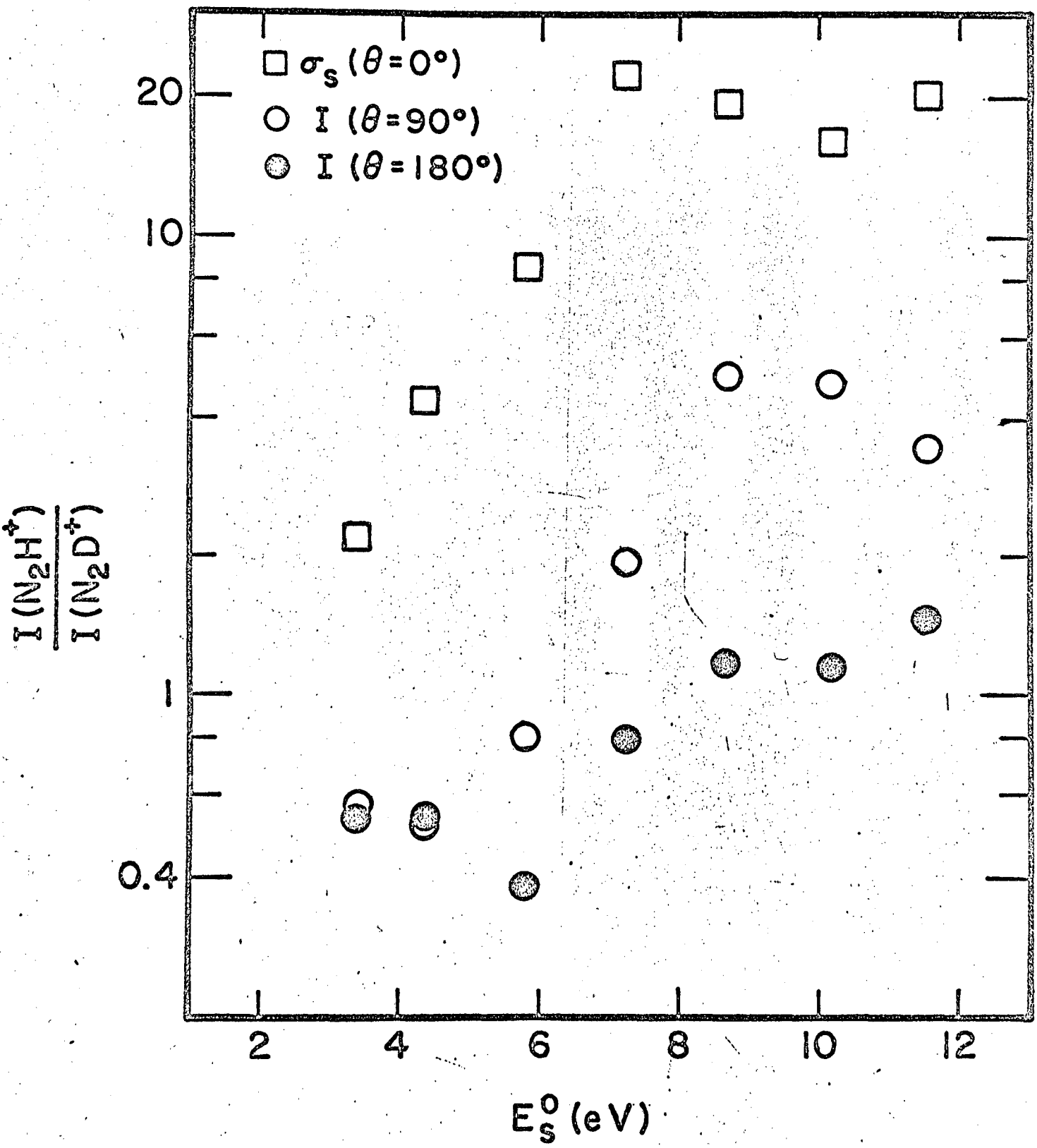
□ $\sigma_s(\theta=0°)$
○ I ($\theta=90°$)
● I ($\theta=180°$)
20
10
1
0.4
$\frac{I(N_2H^+)}{I(N_2D^+)}$
2
4
6
8
10
12
E_s^o (eV)

Figure 9. A map of the normalized intensity $\bar{I}$ of N_2^+ scattered from D_2 at 16.3 eV relative energy in the center of mass coordinate system.

Fig. 9

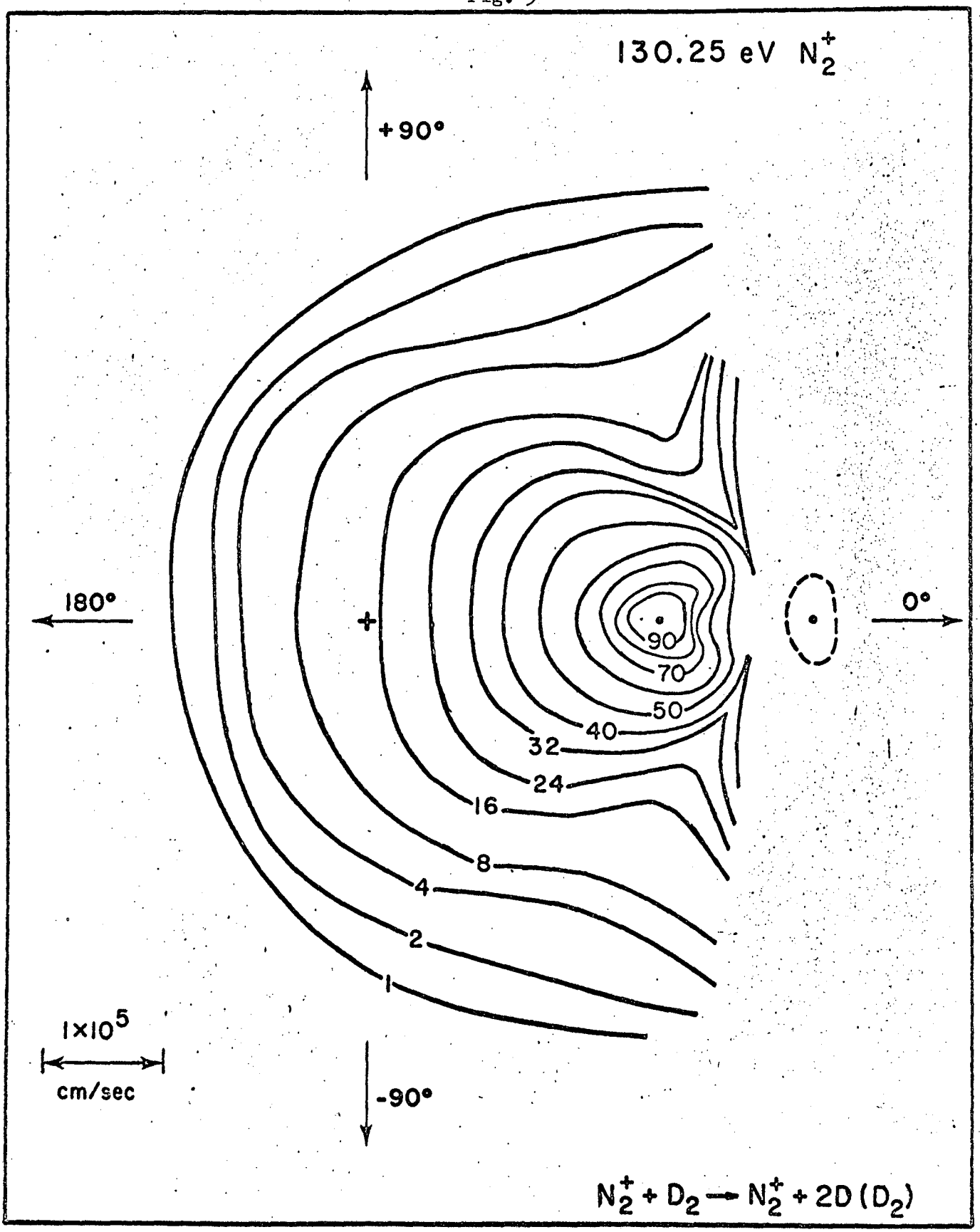
130.25 eV N_2^+
+90°
180°
0°
-90°
90
70
50
40
32
24
16
8
4
2
1
1×10^5
cm/sec
$N_2^+ + D_2 \rightarrow N_2^+ + 2D(D_2)$

Figure 10. The probability P(Q) of finding a relative energy loss Q as a function of Q for N_2^+ scattered from D_2.

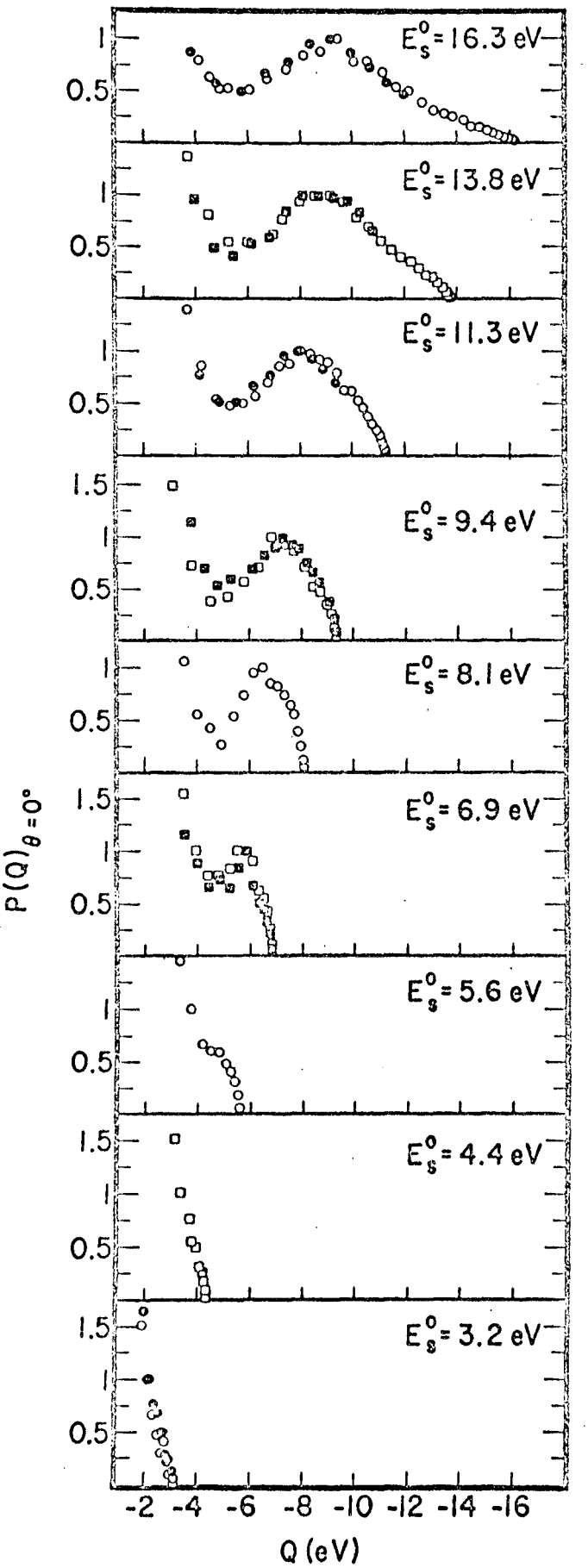
E_s^0 = 16.3 eV
E_s^0 = 13.8 eV
E_s^0 = 11.3 eV
E_s^0 = 9.4 eV
E_s^0 = 8.1 eV
E_s^0 = 6.9 eV
E_s^0 = 5.6 eV
E_s^0 = 4.4 eV
E_s^0 = 3.2 eV
$P(Q)_{\theta=0°}$
Q (eV)
-2 -4 -6 -8 -10 -12 -14 -16
0.5
1
1.5

Fig. 10

Figure 11. The total cross section as a function of relative energy for inelastic scattering with energy loss greater than 4.5 eV for N_2^+ on D_2. Open and closed circles correspond to σ_s from experiments in which the beam energy spread was 1.2 and 0.96 eV FWHM, respectively. The square point is the fully integrated σ calculated from data of Figure 9.

Fig. 11